IEEE Journal of Translational Engineering in Health and Medicine

Received 3 December 2023; revised 2 June 2024 and 19 July 2024; accepted 21 July 2024.
Date of publication 29 July 2024; date of current version 8 August 2024.

Digital Object Identifier 10.1109/JTEHM.2024.3434460

Non-Contact Measurement of Cardiopulmonary Activity Using Software Defined Radios

LEI GUAN[1], XIAODONG YANG[1], (Senior Member, IEEE), NAN ZHAO[1], MALIK MUHAMMAD ARSLAN[1], MUNEEB ULLAH[1], QURAT UL AIN[1], ABBAS ALI SHAH[1], AKRAM ALOMAINY[2], (Senior Member, IEEE), AND QAMMER H. ABBASI[3,4], (Senior Member, IEEE)

[1]Key Laboratory of High Speed Circuit Design and EMC of Ministry of Education, School of Electronic Engineering, Xidian University, Xi'an, Shaanxi 710071, China
[2]School of Electronic Engineering and Computer Science, Queen Mary University of London, E1 4NS London, U.K.
[3]James Watt School of Engineering, University of Glasgow, G12 8QQ Glasgow, U.K.
[4]Artificial Intelligence Research Centre, Ajman University, Ajman, United Arab Emirates

CORRESPONDING AUTHORS: X. YANG (xdyang@xidian.edu.cn) and N. ZHAO (nan_zhao_@hotmail.com)

This work was supported in part by the National Natural Science Foundation of China under Grant 61671349 and Grant 62201413, in part by the Natural Science Basic Research Program of Shaanxi under Grant 2022JQ-666, and in part by the Innovation Capability Support Program of Shaanxi under Grant 2021TD-07.

ABSTRACT Vital signs are important indicators to evaluate the health status of patients. Channel state information (CSI) can sense the displacement of the chest wall caused by cardiorespiratory activity in a non-contact manner. Due to the influence of clutter, DC components, and respiratory harmonics, it is difficult to detect reliable heartbeat signals. To address this problem, this paper proposes a robust and novel method for simultaneously extracting breath and heartbeat signals using software defined radios (SDR). Specifically, we model and analyze the signal and propose singular value decomposition (SVD)-based clutter suppression method to enhance the vital sign signals. The DC is estimated and compensated by the circle fitting method. Then, the heartbeat signal and respiratory signal are obtained by the modified variational modal decomposition (VMD). The experimental results demonstrate that the proposed method can accurately separate the respiratory signal and the heartbeat signal from the filtered signal. The Bland-Altman analysis shows that the proposed system is in good agreement with the medical sensors. In addition, the proposed system can accurately measure the heart rate variability (HRV) within 0.5m. In summary, our system can be used as a preferred contactless alternative to traditional contact medical sensors, which can provide advanced patient-centered healthcare solutions.

INDEX TERMS OFDM, heartbeat estimation, VMD, SVD.

I. INTRODUCTION

VITAL signs such as breathing and heartbeat reflect people's health status. Instabilities in heart rate and breathing rate, both short-term and long-term, are early indicators of physiological changes. Additionally, some diseases can be prevented and detected through the monitoring of abnormalities in vital signs, such as chronic obstructive pulmonary disease (COPD) [1] and sleep apnea [2]. However, due to the limited availability of medical resources, long-term hospitalization is not a viable option for patients. Consequently, there is a pressing need for a continuous and cost-effective method of monitoring vital signs within a home setting.

Wearable devices such as electrocardiograms (ECG) and smartwatches [3] are capable of providing medical-grade insights, yet they may not be suitable for individuals with sensitive skin, such as the burn patients and patients with dermatological conditions. While computer vision-based systems [4], [5], [6] facilitate non-contact monitoring, they necessitate considerations regarding privacy protection and are affected by lighting conditions. Radio Frequency (RF) sensing methods have successfully addressed these constraints. Owing to their non-invasive and privacy-preserving properties, RF sensing has promising clinical applications, from early disease detection to personalized patient care [7].

IEEE Journal of Translational Engineering in Health and Medicine

In radio frequency sensing, radar and ubiquitous signals (such as WiFi) are often used for vital sign monitoring frequency modulated continuous wave (FMCW) [8], [9], [10] radar and ultrawideband (UWB) radar [11] can acquire range bin for the target of interest and suppress interference from other range bins. However, the high cost of dedicated radar hardware is not easy to popularize in the home scene. In recent years, researchers have used communication signals for sensing applications. The main reason is that the frequencies and waveforms used are ubiquitous in common communication equipment, making it possible to implement such a system at a very low cost. AbdeInasser et al. proposed using the received signal strength (RSS) from WiFi for breath detection [12]. However, RSS is insensitive to the minute chest movements during respiration and can be easily overwhelmed by noise [13]. Compared with RSS, the fine-grained channel state information (CSI) in orthogonal frequency division multiplexing (OFDM) systems characterizes the rich changes in signal propagation, e.g., CSI amplitude [14], [15], [16] and CSI phase difference between two antennas [17]. However, due to the influence of multipath, the respiratory waveform patterns collected by users at different positions are quite different, which makes the amplitude and phase difference data difficult to accurately represent the chest displacement. In order to overcome the above problems, some studies [18], [19] discovered the complementarity of CSI amplitude and phase difference, and the comprehensive changes in amplitude and phase difference can accurately estimate respiratory rate (RR). In addition, CSI is composed of multiple subcarriers and different subcarriers have different sensitivity to environmental changes. In [20], Gu et al. extracted the subcarrier with the highest variance to monitor user breathing, but this method may be interfered by ambient noise. In [21] and [22], the principal component analysis method is applied to reduce the dimensionality and noise of subcarriers. However, the extraction of principal component is experiment-based and lacks of theoretical justification.

Heartbeat signals are easily submerged in environmental noise and respiratory harmonics, so it is challenging to extract heartbeat from CSI. In [23], Liu et al. used directional antennas instead of omnidirectional antennas to direct the beam toward the human chest, thus verifying the feasibility of CSI measurement of heart rate (HR). However, this method lacks theoretical validation. Zhang et al. calculated the respiratory signal and heartbeat signal-to-noise ratio (SNR) of each subcarrier, utilized the complementarity of amplitude and phase, and selected subcarriers with high SNR to achieve heart rate monitoring [24]. However, the band-pass [23], [24], [25], [26] filter to extract heartbeat signal may lead to the distortion of the recovered heartbeat signal. Wang et al. successfully obtained human respiratory and heartbeat signals from phase differences using wavelet decomposition [27]. However, the above methods only eliminate the zero-frequency components of phase difference or amplitude, ignoring the DC components of I/Q and static clutter. Therefore, the vital signs may be distorted, which makes it difficult to extract HRV parameters.

The programmable concept of the software defined radio (SDR) provides flexibility in developing the realization and modification of the sensing system. SDR allows us to change various parameters in real-time, such as the number of subcarriers, carrier frequency, bandwidth, and power level for example, the author in [28], [29] extracted CSI by SDR and realized abnormal breath recognition by machine learning. Deep learning [30], [31], [32], [33], [34] and optimization algorithms [35] can help improve recognition accuracy.

To improve the SNR of vital monitoring, we designed a non-contact cardiopulmonary activity sensing system based on OFDM using a SDR platform. The proposed system has the advantages of miniaturization, high sensitivity and non-invasive, which can meet the needs of clinical applications. Specifically, we propose the SVD method to achieve noise reduction and dimension reduction, which is verified by theory and experiment. In addition, this study reveals the influence of static components on CSI phase. We estimate the static component by circle fitting method, which improves the SNR of vital signs. We modified the VMD method to ensure the extraction of heartbeat signals, and the experimental results show that the proposed method is better than the existing methods in heart rate (HR) estimation. In summary, our system is helpful for the analysis of respiratory and heartbeat rhythm, detection of HRV parameters, and clinical cardiopulmonary disease evaluation.

The main contributions of this paper are summarized as follows:

1. We propose using SVD method to achieve denoising and dimensionality reduction of CSI, which makes it possible to extract vital signs under low SNR conditions.
2. We propose using the l_1-norm to estimate the DC component in CSI. After DC compensation, the modified differentiate and cross-multiply (MDACM) is further used to obtain accurate phase of vital sign signals.
3. We modified VMD to separate respiratory and heartbeat signals. In addition, we can accurately obtain parameters of HRV from the separated heartbeat signal. The experimental results show that our system has high consistency with the medical sensors.

The remaining of this paper is organized as follows: Section II presents the system architecture and signal model. Section III presents proposed method and signal processing, include frame synchronization, SVD filtering, DC offset calibration, phase demodulation and vital signs signal separation. Section IV presents simulation and experimental results, performance evaluation and analysis. Finally, conclusions are presented in Section V.

II. ARCHITECTURE AND MODEL

In this section, we will introduce the architecture of the system in detail.

A. SYSTEM ARCHITECTURE

The system architecture is shown in Fig. 1. The low cost, flexible universal software radio peripheral (USRP) B210 software defined radio (SDR) is used as a transceiver. The microstrip directional antenna with a gain of 14 dBi is used to transmit and receive RF signals, and its horizontal and vertical beamwidth are 35° and 40°, respectively. This wide beamwidth can illuminate a larger field, which allows the target to have some slight misalignment relative to the antenna. The implemented hardware is shown in Fig. 2. We design OFDM flow graph in open source GNUradio framework and deploy it on USRP B210 to CSI in real time.

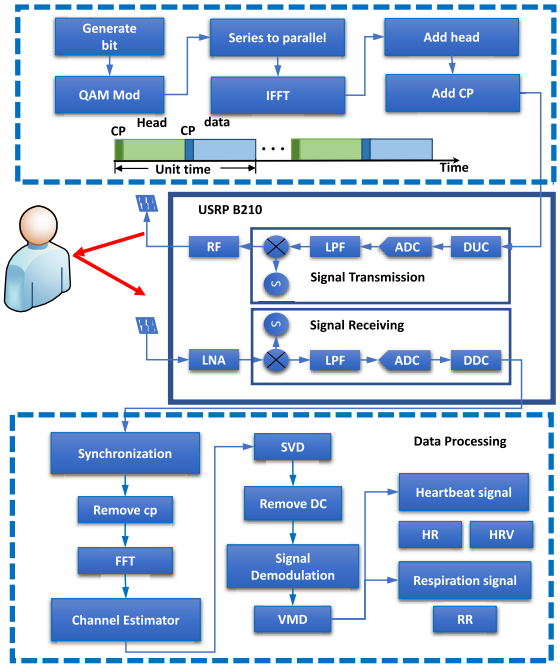

FIGURE 1. System architecture.

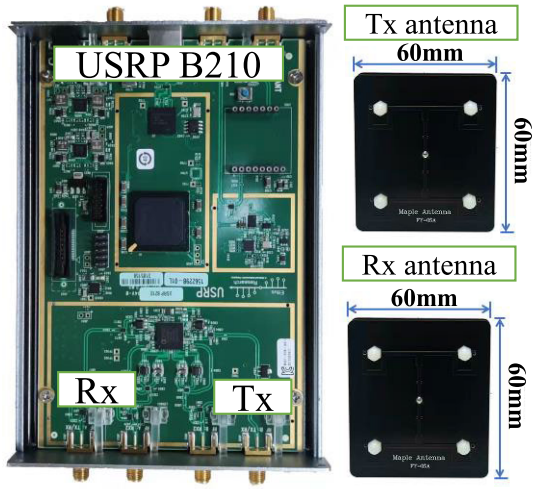

FIGURE 2. Hardware for sensing system.

In the transmitting module, we use Matlab 2022a to generate baseband signals. Each frame consists of two parts: head and data. The head part is used for frame synchronization. The data part is an OFDM symbol used for sensing, which is converted to the time domain by an inverse fast Fourier transform (IFFT) of length 64. Further, a cyclic prefix (CP) of size 8 samples is appended to each part, making each part 72 samples long.

In the receiving module, frame synchronization is performed using the head part, and then CP and head are further removed from the received signal. After performing fast Fourier transform (FFT) on the remaining data part, the frequency domain information of 64 subcarriers can be obtained. We use SVD to remove non-stationary noise and reduce the dimensionality of 64 subcarriers. It is worth noting that vital sign information mainly depends on the phase of the RF signal rather than its amplitude. Compressed sensing is used to remove the DC component, and then demodulate the signal to obtain the phase variation. Finally, the modified VMD to decompose the phase to obtain the target's breathing and heartbeat signals.

B. SIGNAL MODEL

The movement of the chest wall caused by breathing and heartbeat causes periodic changes in RF signals. The phase variation of the Rx signal can characterize the target's cardiorespiratory activity. Let R_0 be the distance between antenna and human body. $R_v(t)$ represents the displacement of the chest caused by respiration and heartbeat. The instantaneous distance $R(t)$ from the sensing system to the human body is expressed as

$$\begin{aligned} R(t) &= R_0 + R_v(t) \\ &= R_0 + A_b \sin(2\pi f_b t) + A_h \sin(2\pi f_h t + \Delta\theta) \end{aligned} \tag{1}$$

where A_b and A_h are the amplitudes of respiration and heartbeat, respectively, f_b and f_h are the frequencies of respiration and heartbeat, respectively, and the $\Delta\theta$ represents the phase difference between respiration and heartbeat at the initial moment. The Channel frequency response (CFR) can be decomposed into dynamic components $H_d(q,t)$, static components H_s, and noise n. Therefore, the Rx signal is expressed as:

$$H(q,t) = \underbrace{a_v e^{-j2\pi(f+q\Delta f)\tau_v(t)}}_{H_d(q,t)} + \underbrace{\sum_{l=1}^{L} a_l e^{-j2\pi(f+q\Delta f)\tau_l}}_{H_s} + n \tag{2}$$

where a_v and $\tau_v(t) = \frac{2R(t)}{c}$ are the amplitude and delay of the human body's reflected signal, respectively, a_l and τ_l are the amplitude and delay of the lth path, respectively, f is the carrier frequency of the wireless signal, Δf is the interval between subcarriers, q is the index of the subcarrier, and n is noise.

Previous study [34] have shown that the coupling/leakage from Tx to Rx accounts for a large portion of the total received RF power. In order to simplify the analysis, the coupling signal is considered as the static components. The power of the static and dynamic components can be expressed as

$$|H_s|^2 = P_t - ISO \tag{3}$$

$$|H_d(q,t)|^2 = \frac{P_t G_t G_r \lambda^2 \sigma}{R^4 (4\pi)^3} \tag{4}$$

where P_t is the Tx power, ISO is the Tx-Rx isolation, G_r and G_t represent the gain of the Rx and Tx antennas, respectively, λ represents the wavelength, σ is radar cross section (RCS). The static signal (DC) affects the phase of vital sign signals. Therefore, it is necessary to analyze the signal intensity of the static and dynamic components in order to obtain accurate vital sign signals, the ratio of static component power to dynamic component power is expressed as

$$\rho = \frac{|H_d|}{|H_s|} = \sqrt{\frac{ISO \times G_t G_r \lambda^2 \sigma}{R^4 (4\pi)^3}} \tag{5}$$

We will explain ρ influence on the phase in the following two cases:

In case 1, the intensity of the dynamic component is greater than that of the static component, i.e., $\rho > 1$. When the dynamic component H_d rotates for one cycle, the phase change of the received signal is 2π as shown in Fig. 3(a). In this case, the phase change caused by target motion is as large as possible.

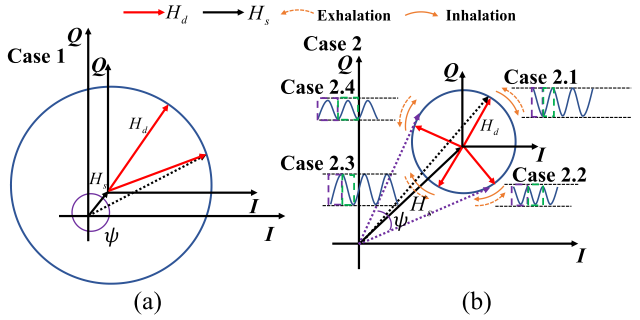

FIGURE 3. Illustration of the phase change under different cases. (a) case1: the phase change when $\rho > 1$. (2) case2: the phase change when $\rho < 1$.

In case 2, the intensity of the reflected signal is less than or equal to that of the static component. We further subdivide this case into four cases as shown in Fig. 3(b). The purple box and the green box represent the exhalation and inhalation, respectively. In case 2.1, the phase decreases during inspiration and increases during expiration. In case 2.2, the phases of inspiration and expiration decrease first and then increase, which makes the waveform of one respiratory cycle approximate to the cosine of two cycles. The respiratory rate (RR) estimation method based on peak detection is ineffective in case 2.2. The phase change in case 2.3 is opposite to case2.1, and the phase change in case 2.4 is opposite to case2.2. In summary, it is difficult to effectively distinguish between exhalation and inhalation from the shape of the waveform and accurately estimate rhythm when ρ<1. In the study, the distance between Tx antenna and Rx antenna is 15cm, the *ISO* measured by vector network analyzer is 38 dB. The RCS of an adult chest wall is about 0.1 at 5.8 GHz [37]. After converting the antenna gain and *ISO* into linear values and inserting them into (5), ρ is equal to 1 when $R = 0.85$ m.

III. METHODOLOGY

A. FRAME SYNCHRONIZATION

In order to correctly receive the reflected signal of the target, the OFDM receiver need to performs synchronization. In OFDM systems, the phase of the Rx signal is affected by the carrier frequency offset (CFO), sampling frequency offset (SFO), and packet detection delay (PDD). The CFO and SFO are caused by the asynchronous hardware of the transceiver equipment. We use one USRP to transmit and receive signals to avoid the influence of the CFO and SFO. The frame header is Minn timing synchronization sequence, and its autocorrelation function has sharp peaks, which improves the accuracy of frame synchronization [38]. The detailed frame structure is shown in Fig.4.

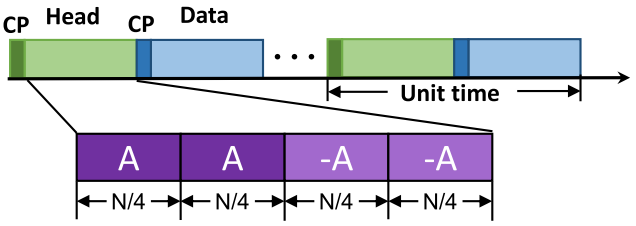

FIGURE 4. Diagram of frame structure.

The A is the basic block of the training sequence and N is the number of subcarriers. The samples of the synchronization sequence are designed to be of the form [A, A, −A, −A]. The decision function is as follows:

$$p(d) = \sum_{k=0}^{1} \sum_{m=0}^{\frac{N}{4}-1} y^* \left(d + m + \frac{Nk}{2}\right) y \left(d + m + \frac{Nk}{2} + \frac{N}{4}\right) \tag{6}$$

where $P(d)$ represents the accumulation result, d represents the starting position of the sampling point, and y represents the received signal. The total energy of the training sequence is expressed as:

$$E(d) = \sum_{k=0}^{1} \sum_{m=0}^{\frac{N}{4}-1} \left| y \left(d + m + \frac{N}{4} + \frac{Nk}{2}\right) \right|^2 \tag{7}$$

The maximum likelihood estimate of the ideal sampling point is expressed as:

$$d = \arg\max_d \frac{|p(d)|}{E(d)} \tag{8}$$

However, the CP with length $N/4$ will cause the Minn timing method to fail. Therefore, we set the CP length to $N/8$ =8.

B. CHANNEL ESTIMATION

After synchronization, we remove the head and CP to get the data part. The data part data is converted to parallel, and then FFT of length N is performed. After the above processing, we can get the frequency domain signals $\mathbf{Y}(t) = [Y(1, t), Y(1, t),\ldots, Y(N, t)]$. The channel frequency response $H(q, t)$ can be obtained by dividing the received signal from the transmitted signal.

$$H(q,t) = \frac{Y(q,t)}{X(q,t)} \tag{9}$$

where $X(q, t)$ is the data part transmitted by the transmitter. Rewrite $H(q, t)$ to matrix form to obtain the channel frequency response matrix $\mathbf{H}$:

$$\mathbf{H} = \begin{bmatrix} H(1,1) & H(1,2) & \cdots & H(1,T) \\ H(2,1) & H(2,1) & \cdots & H(2,T) \\ \vdots & \vdots & \ddots & \vdots \\ H(N,1) & H(N,2) & \cdots & H(N,T) \end{bmatrix} \tag{10}$$

C. SVD FOR NON-STATIONARY CLUTTER SUPPRESSION

The received signal matrix $\mathbf{H}$ contains multiple subcarriers and is inevitably affected by noise. We propose using SVD to achieve dimensionality reduction and noise suppression of the matrix $\mathbf{H}$. The SVD can be presented as

$$\mathbf{H} = \mathbf{U}\Sigma\mathbf{V} = \sum_{i=1}^{K} \mathbf{u}_i \boldsymbol{\sigma}_i \mathbf{v}_i^T \tag{11}$$

where $\mathbf{U} = [\mathbf{u}_1, \mathbf{u}_2, \ldots, \mathbf{u}_N]$ and $\mathbf{V} = [\mathbf{v}_1, \mathbf{v}_2, \ldots, \mathbf{v}_T]$ are the matrices of empirical orthogonal functions and the matrix of principal components, respectively, namely $\mathbf{U}^T\mathbf{U} = \mathbf{I}$, $\mathbf{V}\mathbf{V}^T = \mathbf{I}$. $\mathbf{u}_k \in \mathbb{C}^{N\times 1}$, $\mathbf{v}_k \in \mathbb{C}^{T\times 1}$. Notice that $N \leq T$, $\boldsymbol{\Sigma}\ \boldsymbol{\mathcal{D}}\ [\boldsymbol{\Lambda}\mathbf{0}]$ is the diagonal matrix of eigenvalues, with $\boldsymbol{\Lambda} = diag(\sigma_1, \sigma_2, \ldots, \sigma_K)$. σ_i is the singular values sorted in the descending order. Rewrite (2) with vector notation:

$$\begin{aligned} \mathbf{H} &= \mathbf{H_s} + \mathbf{H_d} + \mathbf{n} \\ &= \underbrace{\sum_{l=1}^{L} \boldsymbol{\sigma}_l \mathbf{u}_l \mathbf{v}_l^T}_{①} + \underbrace{\boldsymbol{\sigma}_s \mathbf{u}_s \mathbf{v}_s^T}_{②} + \underbrace{\sum_{r=1}^{R} \boldsymbol{\sigma}_r \mathbf{u}_r \mathbf{v}_r^T}_{③} \end{aligned} \tag{12}$$

The structure of (12) is similar to that of SVD (11). The item ① is the signal with high correlation and energy, including leakage signal and reflection signals from static objects which affect the sensitivity of the receiver. The item ② is the vital sign signal. The item ③ is the noise. By observing (11) and (12), it can be found that the $\mathbf{V}$ contains the reflected signal of the target of interest. According to the analysis in Section II-B, when the target reflected signal is larger than the static signal, i.e., $\sigma_s > \sigma_l > \sigma_r$, the first column $\boldsymbol{v}_1$ in $\mathbf{V}$ contains human respiration and heart rate signals. When the static signal is larger than the target reflected signal, i.e., $\sigma_l > \sigma_s > \sigma_r$, the $L+1$ column of $\mathbf{V}$ contains the target's vital signs. Due to the limitation of OFDM bandwidth, it is difficult for receivers to separate static and dynamic components. In other words, the eigenvector corresponding to the first non-zero singular value contains the human body reflection signal and the static signal. The remaining eigenvectors are noise. Therefore, (12) should be rewritten as follows

$$\mathbf{H} = \mathbf{u}_s' \boldsymbol{\sigma}_s' \mathbf{v}_s'^T + \sum_{r=1}^{R} \boldsymbol{\sigma}_r \mathbf{u}_r \mathbf{v}_r^T \tag{13}$$

After SVD on $\mathbf{H}$, the first column $\mathbf{v}_1$ in $\mathbf{V}$ is extracted to reconstruct vital sign signals. It can be found that SVD not only reduces the dimension of carrier, but also suppresses clutter interference.

D. DC OFFSET CALIBRATION AND PHASE DEMODULATION

The vital signs signal appears as an arc on the I/Q complex plane. Due to the presence of DC, the center of the arc will deviate from the origin. In addition, DC offset will lead to serious distortion of the phase information and an inaccurate measurement result. Considering the DC offset dc_I/dc_Q, the I/Q signals of $\mathbf{v}_1$ can be given by

$$I(i) = A_I \cos\left(\frac{4\pi R_v(i)}{\lambda} + \theta + \Delta\phi(i)\right) + dc_I \tag{14}$$

$$Q(i) = A_Q \sin\left(\frac{4\pi R_v(i)}{\lambda} + \theta + \Delta\phi(i)\right) + dc_Q \tag{15}$$

where $\Delta\phi(n)$ is residual noise, $A_I(t)$ and $A_Q(t)$ are the amplitudes in channel I and channel Q. DC offset estimation can be formulated into a circle fitting problem. The state-of-the-art method for this problem is to relax the residual d_i

$$d_i = (I(i) - a)^2 + (Q(i) - b)^2 - r^2 \tag{16}$$

where r the radius of the fitted circle, a and b denote the DC in the I and Q channels. The l_2-norm takes into account all the measured values and outliers, resulting in a large error in the estimated DC. To improve measurement accuracy, the l_1-norm minimization is used for calibrating DC offset

$$\min \|\mathbf{d}\|_{l_1} = \min \|\mathbf{A}\mathbf{x} - \boldsymbol{y}\|_{l_1} \tag{17}$$

where $\boldsymbol{d} = [d_1, d_2,\ldots, d_N]^T$,

$$\mathbf{A} = \begin{bmatrix} 2I(1) & 2Q(1) & 1 \\ . & . & . \\ . & . & . \\ . & . & . \\ 2I(N) & 2Q(N) & 1 \end{bmatrix}, \quad \boldsymbol{x} = \begin{bmatrix} a \\ b \\ r^2 - a^2 - b^2 \end{bmatrix},$$

$$\boldsymbol{y} = \begin{bmatrix} I(1)^2 + Q(1)^2 \\ . \\ . \\ . \\ I(N)^2 + Q(N)^2 \end{bmatrix} \tag{18}$$

It can transform (17) into a non-constrained and non-differentiable optimization problem. We use CVX toolbox to

IEEE Journal of Translational Engineering in Health and Medicine

solve the above problem. The I/Q signals after eliminating DC is represented as

$$I'(i) = I(i) - a \tag{19}$$
$$Q'(i) = Q(i) - b \tag{20}$$

After eliminating DC, we adopt the MDACM algorithm [37] to the synthesized I/Q signals to solve the phase ambiguity issue. The MDACM only uses the first-order differential operation and avoid the sum of squares of I/Q signals, which improve the linearity and stability. In the digital domain, the MDACM algorithm can be expressed as

$$\varphi(i) = \frac{\lambda}{4\pi} \sum_{m=2}^{i} I'(m-1)Q'(m) - I'(m)Q'(m-1) \tag{21}$$

E. RESPIRATION AND HEARTBEAT EXTRACTION ALGORITHM

The respiratory and heartbeat signals are quasi periodic signals with relatively stable periods, which can be regarded as several baseband signals. The signals related to the human subject are sparse in the frequency domain, so there are K signals with frequency ω_k to reconstruct the respiration and heartbeat signals [40]. We use VMD [41] to decompose $\varphi(i)$ into discrete number of sub signals (IMF) with sparsity in the frequency domain. For each mode μ_k, the corresponding one-sided spectrum of the analytical signal is obtained by Hilbert transform, and then multiplied by a complex exponential function with the respective estimated center frequency as a parameter to adjust the mode spectrum to the baseband. Finally, the bandwidth is estimated by H^1 Gaussian smoothing of the demodulation function. Therefore, it can be described as

$$\min_{\{\mu_k\},\{\omega_k\}} \left\{ \sum_{k=1}^{K} \left\| \partial t \left(\left(\delta(t) + \frac{j}{\pi t} \right) * \mu_k(t) \right) e^{-j\omega_k} \right\|_2^2 \right\}$$
$$\text{s.t.} \sum_k \mu_k = \varphi \tag{22}$$

where $\{\mu_k\} = \mu_1, \mu_2, \ldots \mu_K, \{\omega_k\} = \omega_1, \omega_2, \ldots \omega_K$ are all modes and their corresponding center frequencies, respectively. In order to reconstruct $\{\mu_k\}$ and $\{\omega_k\}$ under constraint conditions, a quadratic penalty term α and Lagrange multiplier λ are introduced based on the (22). Therefore, the augmented Lagrange function obtained is as follows

$$L(\{\mu_k\}, \{\omega_k\}, \lambda) = \alpha \sum_k \left\| \partial t \left(\left(\delta(t) + \frac{j}{\pi t} \right) * \mu_k(t) \right) e^{-j\omega_k} \right\|_2^2 + \left\| f(t) - \sum_k \mu_k(t) \right\|^2 + \left\langle \lambda(t), f(t) - \sum_k \mu_k(t) \right\rangle \tag{23}$$

where α increases the reconstruction fidelity in the form of independent and identically distributed Gaussian noise, and its weight is inversely proportional to the noise level. Given K, α and λ, the optimization problem of the above formula can be solved iteratively by using ADMM to update $\hat{\mu}_k^{n+1}$, $\hat{\omega}_k$ and $\hat{\lambda}^{n+1}$ iteratively. By using FFT to update $\hat{\mu}_k^{n+1}$, the modal function in the frequency domain can be expressed as follows

$$\mu_k^{n+1}(\omega) = \frac{f(\omega) - \sum_{i \neq k} \mu_i(\omega) + \frac{\lambda(\omega)}{2}}{1 + 2\alpha(\omega - \omega_k)^2} \tag{24}$$

where n is the iteration index, $\hat{f}(\omega)$ and $\hat{\mu}_i(\omega)$ are Fourier transform of input signal $f(x)$ and kth modes $\mu_k(t)$, respectively.

The update expression of the center frequency is as follows:

$$\omega_k = \frac{\int_0^\infty \omega |\mu_k(\omega)|^2 d\omega}{\int_0^\infty |\mu_k(\omega)|^2 d\omega} \tag{25}$$

The Lagrange multiplier operator $\hat{\lambda}^n$ is updated as:

$$\lambda^{n+1} \leftarrow \lambda^n + \tau \left(f \left(\omega - \sum_k \mu_k^{n+1}(\omega) \right) \right) \tag{26}$$

The iteration termination condition is:

$$\sum_k \frac{\left\| \mu_k^{n+1} - \mu_k^n \right\|_2^2}{\left\| \mu_k^n \right\|_2^2} < \varepsilon \tag{27}$$

However, the number of decomposition layers K and the penalty value α have a great influence on the performance of VMD. If K is too small, the problem of mode mixing will be caused. On the contrary, it will lead to false modes and increase the amount of calculation. The value of α affects the optimal bandwidth range of the mode. When α is too small, $\hat{\mu}_k$ has a larger search range around the center frequency $\hat{\omega}_k$, thereby introducing unnecessary components. On the contrary, it leads to the loss of useful information.

Algorithm 1 Vital Signs Signal Extraction Algorithm

Input: φ
Output: μ, ω
Initialize:Set K_{min}, K_{max}, α_{min}, α_{step}, α_{max}
for α=α_{min}: α_{step}: α_{max} **do**
  for K= K_{min}: 1: K_{max} **do**
    n= 0;
    repeat
      $n = n+1$;
      for $k = 1: K$ **do**
        update $\hat{\mu}_k$ *using equation*(24);
        update $\hat{\omega}_k$ *using equation*(25);
        update λ^n *using equation*(26);
      end for
    until *convergence: equation*(27) or n>n_{max}
    If*exist* $L\hat{\omega}_k/T \in [f_{h_{\min}}, f_{h_{\min}}]$ **then**
      return μ, ω
    end if
  end for
end for

In order to be able to separate the breathing signal and the heartbeat signal from the signal $\varphi(i)$ of duration T and length L, K and α need to be adaptively changed. In the parameter

optimization algorithm, the mainstream algorithms such as particle swarm optimization algorithm, genetic algorithm and other intelligent optimization algorithms find the optimal parameter combination through the self-defined fitness function. If the number of particles or the size of the population is large, modal decomposition is required every time the fitness function is calculated, which will consume a lot of time. Considering that the vital sign signal components are limited, and the bandwidth of respiration and heartbeat is known. Therefore, the search range of K and α can be fixed to determine appropriate parameters. In addition, we found that it is easier to extract respiratory signals from $\varphi(i)$ compared to extracting heartbeat signals. Once the frequency component of the heartbeat is decomposed, i.e., $f_h \in [f_{h_{min}}, f_{h_{max}}]$, we end the iteration process. Respiration and heartbeat extraction algorithm is shown in Algorithm 1. Considering that the received signal contains breathing, harmonic of breathing, heartbeat, noise, and the incoherent components of the received signal are limited. We set $K_{min} = 5$, $K_{max} = 9$, $\alpha_{min} = 1000$, $\alpha_{setp} = 500$, $\alpha_{max} = 2500$, $f_{h_{min}} = 0.9$ Hz, $f_{h_{max}} = 1.6$ Hz. K_{min} and K_{max} are the minimum and maximum modes of decomposition, respectively. α_{min} and α_{max} are the minimum penalty factor and the maximum penalty factor, with a step size of α_{step}. $f_{h_{min}}$ and $f_{h_{max}}$ are the minimum and maximum frequencies of adult heartbeat, respectively. It should be noted that these hyperparameters are empirical.

IV. EXPERIMENT AND RESULTS

This section introduces the evaluation details of our system, including simulation, practical system implementation, experiment setup and performance analysis.

A. SIMULATION AND RESULTS

Normally, the chest movement caused by heartbeat is 0.2∼0.5 mm with 50∼100 bpm. Whereas, the chest movement caused by respiration is in range several millimeters with 6∼30 bpm. In the simulation, we set the movement of the human chest wall to be a periodic movement, which consists of breathing with a frequency of $f_b = 0.2$ Hz and heartbeat with a frequency of $f_h = 1.5$ Hz. The displacement of the chest wall caused by respiration and heartbeat is $A_b = 2$ mm and $A_h = 0.5$ mm, respectively. The distance between the target and the antenna is 0.8 meters. The gain of the antenna is 14 dB. The carrier frequency of OFDM signal is 5.8 GHz and the bandwidth is 20 MHz. The Fig. 5 shows the results for SNR=20 dB and SNR=2 dB. The signal after SVD filtering and DC compensation is denoted as $\boldsymbol{v}_1$. For multi-carrier modulated OFDM signals, the phases of the non-zero carriers are very similar in morphology. We choose the phase of the 7th sub-carrier as the raw signal for convenience. In the case of SNR =20 dB, it can be clearly seen from the raw signal and $\boldsymbol{v}_1$ that the respiration and heartbeat signals are shown in Fig. 5(a). After processing by the modified VMD, the respiration and heart rate signals are separated from the original signal as shown in Fig. 5(b). The respiration and heart rate estimated using the FFT are consistent with the simulated settings as shown in Fig. 5(c).

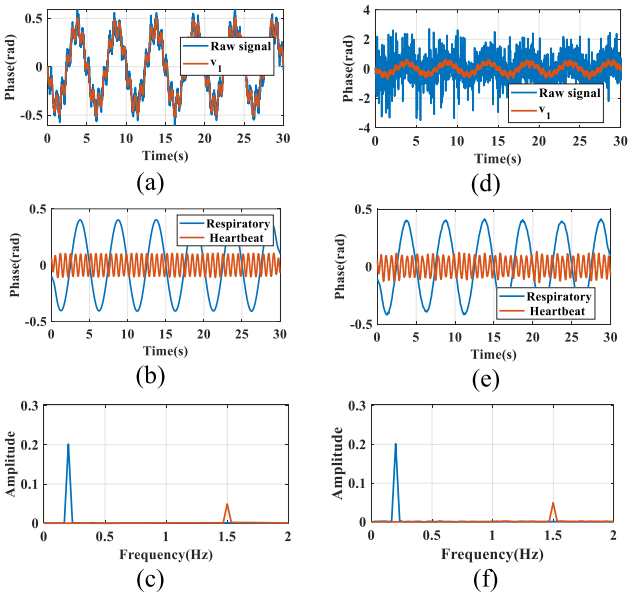

FIGURE 5. Simulation results under different SNR.

In the case of SNR=2 dB, the heartbeat signal cannot be observed from the raw signal. The components extracted by SVD can retain the characteristics of heartbeat and respiration at low SNR as shown in Fig. 5(d). Furthermore, the estimated heart rate and respiration rate are consistent with the simulation settings as shown in Fig. 5(e) and (f).

B. EXPERIMENT SETUP

In this study, a total of 6 volunteers participated in the experiment. All volunteers are around 25 years old and have no cardiopulmonary disease. During the experiment, volunteers wear HKD 10C and HKH 11C to monitor heartbeat and breathing signals as the ground truth, respectively. The experimental setup is shown in Fig. 6. The Tx and Rx antenna adopts a high gain directional antenna (14 dBi), and the beam is directed towards the subject's chest. We collected plenty data at different distances (0.5 m, 0.75 m, 1 m). Each volunteer collected data 7 times at each distance, and each experiment lasted for 30s. The sampling frequencies of HKD 10C and HKH 11C are 200 Hz and 50 Hz, respectively. The subjects remained seated without any major physical movements during data collection. All experiments were performed in a typical office. The proposed system includes a computer and a USRP. The USRP is used to send and receive OFDM signals at 5.8 GHz. In order to ensure that no RF samples are lost between the USB bus and the USRP B210, we set the bandwidth to 100 KHz. The specific parameters are shown in Table 1. This research has been approved by the Medical Ethics Committee of Northwest Women and Children's Hospital, the approval date is May 6th, 2022, and the IRB board protocol number is 2022-013.

IEEE Journal of Translational Engineering in Health and Medicine

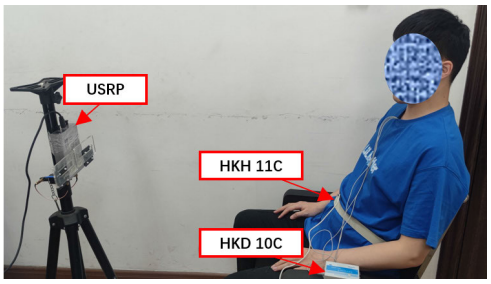

FIGURE 6. The experimental setup.

TABLE 1. Parameter setting.

Parameter	Value
Antenna gain	14 dBi
Center frequency	5.8 GHz
Number of subcarriers	64
CP length	8
Bandwidth	100 KHz
Tx gain	75 dB
Rx gain	75 dB

C. EXTRACTING VITAL SIGNS

The raw signal, filtered signal, and all modes decomposed by the modified VMD are shown in Fig. 7(a). The spectrum of each signal is shown in Fig. 7(b). After SVD filtering and DC compensation, the fluctuations caused by breathing and heartbeat can be seen. Then, the filtered signal is decomposed into 5 modes. IMF1 is the respiration signal, and IMF2 is the heartbeat signal. The remaining modes are noise components with different vibration characteristics.

We found that the envelope of the heartbeat is not stable. We use Hilbert transform to extract the envelope of the heartbeat signal. The heartbeat signal is divided by the envelope to obtain a stable heartbeat waveform. Fig. 8 shows the optimized heartbeat waveform and ECG signal. We can find that the processed heartbeat waveform matches the ground truth. Additionally, we have measured the processing times of the proposed methods. The computations were carried out on a computer with a CPU Intel i7-8700 @ 3.2GHz and 16GB RAM. The data length processed was 30s. Specifically, The SVD processing time was about 1.58s, the DC offset calibration time was 0.4456s, and the VMD processing time was 0.543s.

D. ACCURACY ANALYSIS

The Bland–Altman analysis provided a measure of statistical agreement between the estimated and the reference outputs. The bias (μ) denotes the mean difference between the value estimated from our system and the value calculated using the data obtained from the contact sensor. The σ is the standard deviation of the difference. The 95% limits of agreement are $[\mu - 1.96 \times \sigma, \mu + 1.96 \times \sigma]$.

The subject was seated at a distance of 0.5 m, 0.75 m, 1 m in front of our system and asked to remain as still as possible during the experiment. The Blant-Altman graph of the subjects' HR and RR are shown in Fig. 9(a) and Fig. 9(b). The mean difference between estimated HR and reference HR is 0.0006 bmp, and the σ is 0.833 bpm. The mean difference between estimated RR and reference RR is −0.001 bmp, and the σ is 0.118 bpm. Based on Bland–Altman analysis, the LOA of HR and RR are from −1.75 bpm to 1.75 bpm, and from −0.23 bpm to 0.23 bpm, respectively. Apparently, most of the values lie within the LOA range. The experimental results show that our system has a high consistency with the medical wearable sensor. The detection accuracy at different distances is shown in Fig. 9(c). With the increase of distance, the accuracy will decline slightly. However, the accuracy of HR within 1 m is still higher than 99.2%. It is worth noting that the detection accuracy of our system in both HR and RR is above 99.4% at 0.5 m.

E. HRV MEASUREMENT AND ANALYSIS

The above results show that the proposed system can accurately estimate the HR in a short distance, so we further explore the application of the system in HRV. Based on the separated heartbeat signals, the exact time of each heartbeat is determined by detecting the peak value. In this study, we extracted three commonly used time domain indicators: mean of successive normal B-B intervals (MEAN), the standard deviation of the B–B interval (SDBB) and the root mean square of the successive difference (RMSSD) of two intervals. *IBI* is the time interval between the nth and $(n-1)$th heartbeats. the MEAN, SDNN and RMSSD are determined as

$$MEAN = \frac{1}{N_{IBI}} \sum_{i=1}^{N_{IBI}} IBI(i) \tag{28}$$

$$SDRR = \sqrt{\frac{1}{N_{IBI}} \sum_{i=1}^{N_{IBI}} (IBI\ (i) - MEAN)^2} \tag{29}$$

$$RMSSD = \sqrt{\frac{1}{N_{IBI} - 1} \sum_{i=2}^{N_{IBI}} (IBI(i) - IBI(i-1))^2} \tag{30}$$

Table 2 shows the detection results of HRV for 6 subjects. The distance between the subjects and the sensing system is 0.5 m. We can find that our system can achieve 5.98 ms average error of MEAN, 4.85 ms average error of SDRR, 15.93 ms average error of RMSSD.

F. COMPARE WITH EXISTING METHODS

We compare the proposed method with other decomposition methods or multi-scale analysis methods such as ensemble empirical mode decomposition (EEMD), discrete wavelet transformation (DWT), Empirical Wavelet Transform (EWT), empirical mode decomposition (EMD) to demonstrate the superiority of the proposed method. For DWT, the wavelet coefficients adopt the maximum overlap

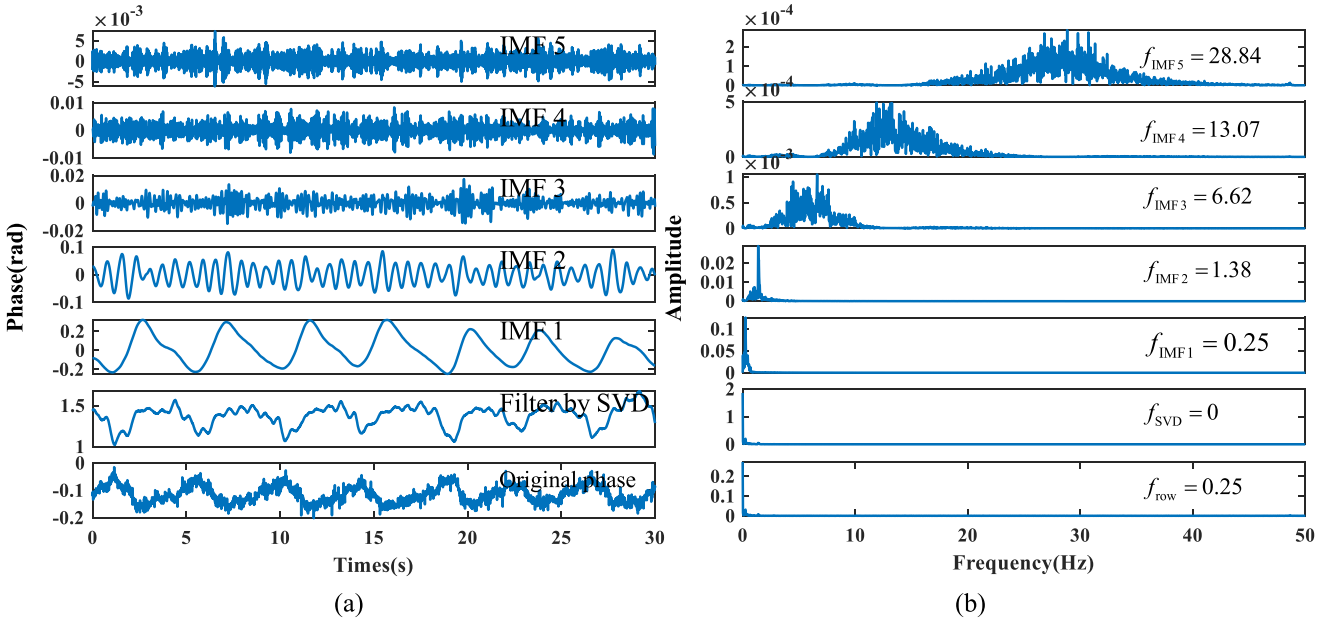

FIGURE 7. Vital sign signal extraction. (a)The original signal, the filtered signal and its decomposition result. (b) The spectrum corresponding to each component.

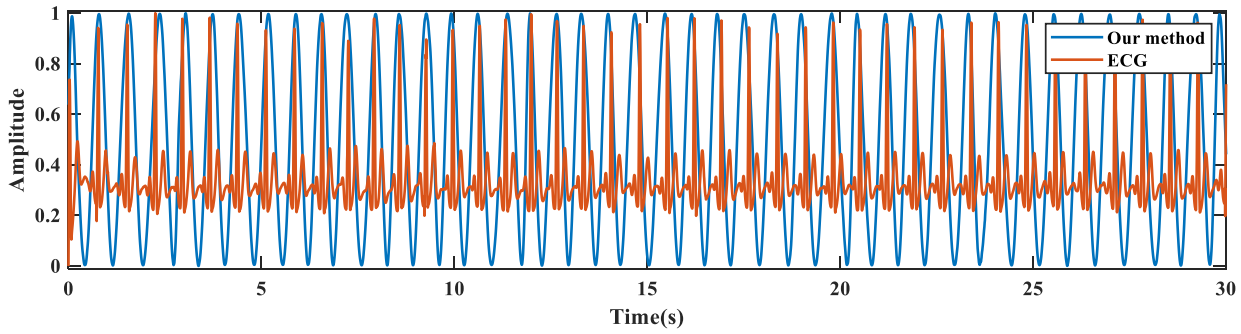

FIGURE 8. ECG signal and extracted heartbeat signal.

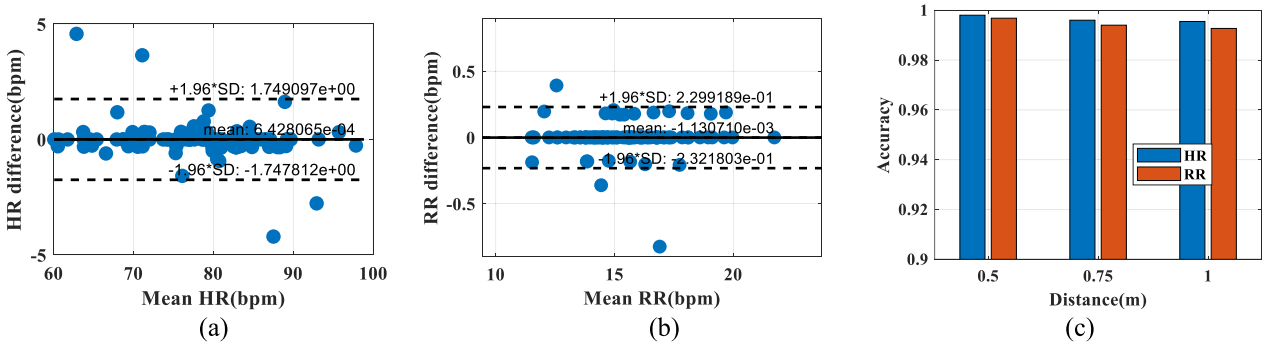

FIGURE 9. (a) Bland–Altman graph for HR. (b) Bland–Altman graph for RR. (c) Accuracy at various distance.

DWT, considering the 7-level decomposition recommended by [42] in order to avoid redundant computation. For EEMD, white Gaussian noise is added to the input signal, and the amplitude of the noise is 0.4 times the standard deviation of the input signal. The cumulative distribution of errors (CDF) for different methods is shown in the Fig. 10. In RR estimation, the performance of EEMD, DWT, EWT, and the proposed method is almost identical as shown in Fig. 10(a).

TABLE 2. Hrv measurements for all subjects.

Subject	MEAN (ms)		SDBB (ms)		RMSSD (ms)	
	ECG	CSI	ECG	CSI	ECG	CSI
1	708.3	707.5	34.1	38.1	34.1	54.7
2	710.9	707.1	26.8	30.5	19.8	34.4
3	770.9	777.8	32.9	40.8	25.1	54.8
4	778.8	761.0	90.7	89.7	12.9	14.1
5	877.9	876.9	54.7	58.5	54.4	75.5
6	959.1	953.5	73.2	62.5	95.3	86.9

In HR estimation, the proposed method is superior to other signal decomposition methods as shown in Fig. 10(b). Due to modal aliasing, EMD has significant errors in estimating RR and HR.

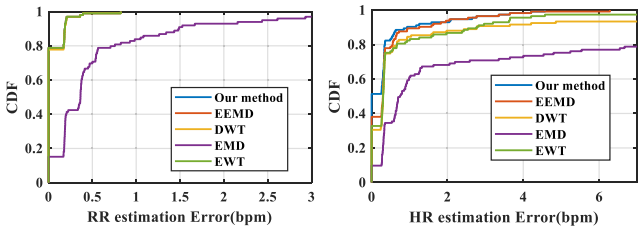

FIGURE 10. Comparison results of state-of-art methods (a) CDF of RR error for all method; (b)CDF of HR error for all method.

V. CONCLUSION

In this paper, we propose a non-contact, high-precision cardiopulmonary activity monitoring system based on OFDM signals. To improve the SNR of measured vital signs, we propose using SVD to remove noise and simultaneously reduce the dimensionality of CSI. To extract undistorted vital sign signals, a circular fitting method is proposed to estimate and compensate the static components. The respiratory and heartbeat signals can be accurately separated from the phase by using the modified VMD. A large number of experiments were performed with 6 volunteers at different distances. The experimental results demonstrate that the proposed method has high consistency with the medical sensor. Moreover, the proposed system can accurately measure HRV indication within 0.5m.

REFERENCES

[1] W. Wang et al., "Millimetre-wave radar-based spirometry for the preliminary diagnosis of chronic obstructive pulmonary disease," *IET Radar, Sonar Navigat.*, vol. 17, no. 12, pp. 1874–1885, Oct. 2023.

[2] X. Yang et al., "Sleep apnea syndrome sensing at C-band," *IEEE J. Transl. Eng. Health Med.*, vol. 6, pp. 1–8, 2018.

[3] D. R. Seshadri et al., "Accuracy of the apple watch 4 to measure heart rate in patients with atrial fibrillation," *IEEE J. Transl. Eng. Health Med.*, vol. 8, pp. 1–4, 2020.

[4] S. Sanyal and K. K. Nundy, "Algorithms for monitoring heart rate and respiratory rate from the video of a user's face," *IEEE J. Transl. Eng. Health Med.*, vol. 6, pp. 1–11, 2018.

[5] K. Zhu, M. Li, S. Akbarian, M. Hafezi, A. Yadollahi, and B. Taati, "Vision-based heart and respiratory rate monitoring during sleep—A validation study for the population at risk of sleep apnea," *IEEE J. Transl. Eng. Health Med.*, vol. 7, pp. 1–8, 2019.

[6] V. Ottaviani et al., "Contactless monitoring of breathing pattern and thoracoabdominal asynchronies in preterm infants using depth cameras: A feasibility study," *IEEE J. Transl. Eng. Health Med.*, vol. 10, pp. 1–8, 2022.

[7] S. Dong et al., "A review on recent advancements of biomedical radar for clinical applications," *IEEE Open J. Eng. Med. Biol.*, early access, May 15, 2024, doi: 10.1109/OJEMB.2024.3401105.

[8] D. Jung, S. Cheon, D. Kim, J. Yoon, and B. Kim, "Short time remote heart rate measurement based on mmWave FMCW radar frame structure," *IEEE Antennas Wireless Propag. Lett.*, vol. 22, no. 6, pp. 1301–1305, Jun. 2023.

[9] B. Zhang, B. Jiang, R. Zheng, X. Zhang, J. Li, and Q. Xu, "Pi-ViMo: Physiology-inspired robust vital sign monitoring using mmWave radars," *ACM Trans. Internet Things*, vol. 4, no. 2, pp. 1–27, May 2023.

[10] Y. Wang et al., "A novel non-contact respiration and heartbeat detection method using frequency-modulated continuous wave radar," *IEEE Sensors J.*, vol. 24, no. 7, pp. 10434–10446, Apr. 2024.

[11] B. Yang, L. Min, M. Wang, and H. Shi, "Non-contact respiratory and heart rate detection using IR-UWB radars under random body activity," *IEEE Trans. Instrum. Meas.*, vol. 73, pp. 1–13, 2024.

[12] H. Abdelnasser, K. A. Harras, and M. Youssef, "UbiBreathe: A ubiquitous non-invasive WiFi-based breathing estimator," in *Proc. 16th ACM Int. Symp. Mobile Ad Hoc Netw. Comput.*, 2015, pp. 277–286.

[13] X. Liu, J. Cao, S. Tang, J. Wen, and P. Guo, "Contactless respiration monitoring via off-the-shelf WiFi devices," *IEEE Trans. Mobile Comput.*, vol. 15, no. 10, pp. 2466–2479, Oct. 2016.

[14] F. Zhang et al., "From Fresnel diffraction model to fine-grained human respiration sensing with commodity Wi-Fi devices," *Proc. ACM Interact., Mobile, Wearable Ubiquitous Technol.*, vol. 2, no. 1, pp. 1–23, Mar. 2018.

[15] P. Kontou, S. B. Smida, and D. E. Anagnostou, "Contactless respiration monitoring using Wi-Fi and artificial neural network detection method," *IEEE J. Biomed. Health Informat.*, vol. 28, no. 3, pp. 1297–1308, Mar. 2024.

[16] F. Han, P. Yang, Y. Feng, W. Jiang, Y. Zhang, and X.-Y. Li, "EarSleep: In-ear acoustic-based physical and physiological activity recognition for sleep stage detection," *Proc. ACM Interact., Mobile, Wearable Ubiquitous Technol.*, vol. 8, no. 2, pp. 1–31, May 2024.

[17] X. Wang, C. Yang, and S. Mao, "PhaseBeat: Exploiting CSI phase data for vital sign monitoring with commodity WiFi devices," in *Proc. IEEE 37th Int. Conf. Distrib. Comput. Syst. (ICDCS)*, Jun. 2017, pp. 1230–1239.

[18] Y. Zeng, D. Wu, R. Gao, T. Gu, and D. Zhang, "FullBreathe: Full human respiration detection exploiting complementarity of CSI phase and amplitude of WiFi signals," *Proc. ACM Interact., Mobile, Wearable Ubiquitous Technol.*, vol. 2, no. 3, pp. 1–19, 2018.

[19] X. Wang, C. Yang, and S. Mao, "Resilient respiration rate monitoring with realtime bimodal CSI data," *IEEE Sensors J.*, vol. 20, no. 17, pp. 10187–10198, Sep. 2020.

[20] Y. Gu, X. Zhang, Z. Liu, and F. Ren, "WiFi-based real-time breathing and heart rate monitoring during sleep," in *Proc. IEEE Global Commun. Conf. (GLOBECOM)*, Dec. 2019, pp. 1–6.

[21] K. Ali, M. Alloulah, F. Kawsar, and A. X. Liu, "On goodness of WiFi based monitoring of sleep vital signs in the wild," *IEEE Trans. Mobile Comput.*, vol. 22, no. 1, pp. 341–355, Jan. 2023.

[22] W. Xie et al., "A real-time respiration monitoring system using WiFi sensing based on the concentric circle model," *IEEE Trans. Biomed. Circuits Syst.*, vol. 17, no. 2, pp. 157–168, Apr. 2023.

[23] J. Liu, Y. Chen, Y. Wang, X. Chen, J. Cheng, and J. Yang, "Monitoring vital signs and postures during sleep using WiFi signals," *IEEE Internet Things J.*, vol. 5, no. 3, pp. 2071–2084, Jun. 2018.

[24] R. Zhang et al., "Hybrid subcarrier selection method for vital sign monitoring with long-term and short-term data considerations," *IEEE Sensors J.*, vol. 22, no. 23, pp. 23209–23220, Dec. 2022.

[25] X. Zhang et al., "Wital: A COTS WiFi devices based vital signs monitoring system using NLOS sensing model," *IEEE Trans. Human-Mach. Syst.*, vol. 53, no. 3, pp. 629–641, Jun. 2023.

[26] I. Shirakami and T. Sato, "Heart rate variability extraction using commodity Wi-Fi devices via time domain signal processing," in *Proc. IEEE EMBS Int. Conf. Biomed. Health Informat. (BHI)*, Jul. 2021, pp. 1–4.

[27] X. Wang, C. Yang, and S. Mao, "On CSI-based vital sign monitoring using commodity WiFi," *ACM Trans. Comput. Healthcare*, vol. 1, no. 3, pp. 1–27, May 2020.

[28] M. Rehman et al., "Contactless small-scale movement monitoring system using software defined radio for early diagnosis of COVID-19," *IEEE Sensors J.*, vol. 21, no. 15, pp. 17180–17188, Aug. 2021.

[29] U. Saeed et al., "Wireless channel modelling for identifying six types of respiratory patterns with SDR sensing and deep multilayer perceptron," *IEEE Sensors J.*, vol. 21, no. 18, pp. 20833–20840, Sep. 2021.

[30] D. Fan et al., "A contactless breathing pattern recognition system using deep learning and WiFi signal," *IEEE Internet Things J.*, early access, Jul. 10, 2024, doi: 10.1109/JIOT.2024.3386645.

[31] H. Zhao, Y. Wu, and W. Deng, "An interpretable dynamic inference system based on fuzzy broad learning," *IEEE Trans. Instrum. Meas.*, vol. 72, pp. 1–12, 2023.

[32] W. Deng, K. Li, and H. Zhao, "A flight arrival time prediction method based on cluster clustering-based modular with deep neural network," *IEEE Trans. Intell. Transp. Syst.*, early access, Dec. 21, 2024, doi: 10.1109/TITS.2023.3338251.

[33] E. Nsugbe, "Toward a self-supervised architecture for semen quality prediction using environmental and lifestyle factors," *Artif. Intell. Appl.*, vol. 10, pp. 35–42, Jan. 2023.

[34] L. Alkhaled, A. Roy, and S. Palaiahnakote, "An attention-based fusion of ResNet50 and InceptionV3 model for water meter digit recognition," *Artif. Intell. Appl.*, Oct. 2023, doi: 10.47852/bonviewAIA32021197.

[35] X. Zhou et al., "Multi-strategy competitive-cooperative co-evolutionary algorithm and its application," *Inf. Sci.*, vol. 635, pp. 328–344, Jul. 2023.

[36] J. Lu, Z. Shao, C. Li, C. Gu, and J. Mao, "A portable 5.8 GHz dual circularly polarized interferometric radar sensor for short-range motion sensing," *IEEE Trans. Antennas Propag.*, vol. 70, no. 7, pp. 5849–5859, Jul. 2022.

[37] E. Piuzzi, P. D'Atanasio, S. Pisa, E. Pittella, and A. Zambotti, "Complex radar cross section measurements of the human body for breath-activity monitoring applications," *IEEE Trans. Instrum. Meas.*, vol. 64, no. 8, pp. 2247–2258, Aug. 2015.

[38] H. Minn, V. Bhargava, and K. Letaief, "A robust timing and frequency synchronization for OFDM systems," *IEEE Trans. Wireless Commun.*, vol. 2, no. 4, pp. 822–839, Jul. 2003.

[39] W. Xu, Y. Li, C. Gu, and J. F. Mao, "Large displacement motion interferometry with modified differentiate and cross-multiply technique," *IEEE Trans. Microw. Theory Techn.*, vol. 69, no. 11, pp. 4879–4890, Nov. 2021.

[40] F. Wang, X. Zeng, C. Wu, B. Wang, and K. R. Liu, "mmHRV: Contactless heart rate variability monitoring using millimeter-wave radio," *IEEE Internet Things J.*, vol. 8, no. 22, pp. 16623–16636, Nov. 2021.

[41] K. Dragomiretskiy and D. Zosso, "Variational mode decomposition," *IEEE Trans. Signal Process.*, vol. 62, no. 3, pp. 531–544, Feb. 2014.

[42] C. Gouveia, D. Albuquerque, P. Pinho, and J. Vieira, "Evaluation of heartbeat signal extraction methods using a 5.8 GHz Doppler radar system in a real application scenario," *IEEE Sensors J.*, vol. 22, no. 8, pp. 7979–7989, Apr. 2022.